Eur. Phys. J. B **32**, 163–176 (2003)
DOI: 10.1140/epjb/e2003-00085-7

THE EUROPEAN PHYSICAL JOURNAL B

Spin polarized current in the ground state of superconductor-ferromagnet-insulator trilayers

M. Krawiec[a], B.L. Györffy, and J.F. Annett

H.H. Wills Physics Laboratory, University of Bristol, Tyndal Ave., Bristol BS8 1TL, UK

Received 23 September 2002 / Received in final form 13 December 2002
Published online 1st April 2003 –

Abstract. We study the ground state properties of a superconductor-ferromagnet-insulator trilayer on the basis of a Hubbard Model featuring exchange splitting in the ferromagnet and electron-electron attraction in the superconductor. We solve the spin-polarized Hartree-Fock-Gorkov equations together with the Maxwell's equation (Ampere's law) fully self-consistently with respect to the order parameter and the current. For certain values of the exchange splitting we find that a spontaneous spin polarized current is generated in the ground state and is intimately related to Andreev bound states at the Fermi level. Moreover, the polarization of the current strongly depends on the band filling.

PACS. 74.50.+r Proximity effect – 74.80.-g Spatially inhomogeneous structures – 72.25.-b Spin polarized transport

1 Introduction

Recently, the proximity effect between a superconductor (SC) and a ferromagnet (FM) has attracted much attention because, due to advances in materials growth and fabrication techniques [1], well controlled structures, in which it can occur became available. Such FM/SC hybrid structures are important from the point of view of their intrinsic scientific interest, as they allow the study of the interplay between ferromagnetism and superconductivity [2] as well as of device applications in such areas of technology as magnetoelectronics [3] or quantum computing [4].

In the present context the proximity, on one hand, means the leakage of superconductivity into the ferromagnet, and on the other, the spin polarization of the superconductor. In normal metal-superconductor systems the proximity effect has been studied over 30 years, and is now well understood [5] to be governed by the Andreev reflection [6] processes, in which an electron at the interface is reflected as a hole while a Cooper pair is transfered into superconductor. This mechanism makes the movement of electrons and holes in the normal metal highly coherent.

If the normal metal is replaced by a ferromagnet a number of new phenomena may occur [7]. For instance one may expect a version of the $FFLO$ state, predicted in the sixties for a bulk superconductor in a strong spin exchange field, by Fulde and Ferrell [8] and Larkin and Ovchinikov [9], to be realized. In the bulk, as is well known, the exchange field tends to polarize the conduction electrons and holes. In particular if these electrons are Cooper paired, naively one would expect that either the exchange field is too weak to break the pairs, or it leads to the first order phase transition to the normal state. However, as was demonstrated in references [8,9], for certain values of the exchange field a new superconducting depairing state is realized through first order phase transition from the BCS state and it transforms continuously, by a second order phase transition, into the normal state as the strength of the exchange field is increased. This $FFLO$ state has a spatially dependent order parameter corresponding to the nonzero center of mass motion of the Cooper pairs. Another novel feature of this state is a current flowing in the ground state. The unpaired electrons tend to congregate at one portion of the Fermi surface so a quasiparticle current is produced. In order to satisfy the Bloch theorem [8]: no current in the ground state, a supercurrent, generated by the nonzero value of the pairing momentum, flows in opposite direction, and the total current is zero.

Interestingly, similar oscillations of the pairing amplitude (Cooper pair density) have been predicted [10–13] in a ferromagnet proximity coupled to a superconductor. It turns out that these oscillations are responsible for the oscillatory dependence of the critical temperature on the thickness of the ferromagnetic slab [11,12]. This effect as well as the corresponding oscillations of the density of states at the Fermi level [15,16], have been observed experimentally [14,17]. In this paper we investigate further the ramifications of these interesting phenomena.

One of these is the formation of so called π junction state [18] which is also a fingerprint of the oscillatory

[a] e-mail: m.a.krawiec@bristol.ac.uk

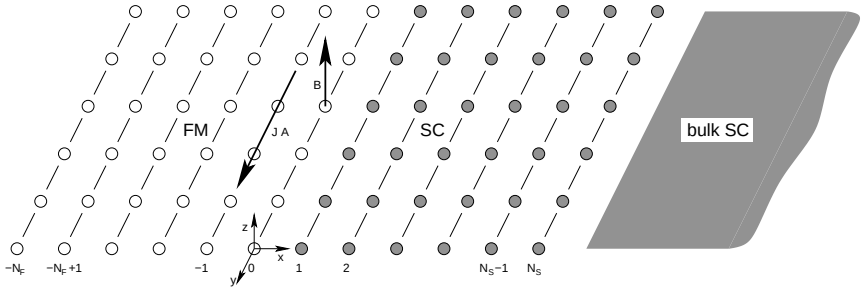

Fig. 1. Schematic view of the (finite thickness) ferromagnet-semi-infinite superconductor heterostructure. Directions of the magnetic field (B) as well as vector potential (A) and current (J) are indicated.

behaviour of the pairing amplitude. The π-state effect has been extensively studied in connection with the high-T_c and other exotic superconductors, where due to spatial inhomogeneity of the order parameter, the Cooper pair wave function can change sign at the interface and this leads to the formation of a zero-energy mid-gap state. Remarkably, this zero-energy state is unstable to the occurrence of a spontaneous current flowing parallel to and within a coherence length of the interface (see *eg.* [19–21] and references therein). In what follows we report on our finding similar spontaneous currents but of different origin in a $SC/FM/I$ trilayer.

We also find zero energy bound states due to the finite size of the FM slab. In fact even for a N/SC heterostructure, in agreement with [22], we have found states within the SC gap. Although the energy of these states depend on the thickness of the normal metal, they never reach zero, namely ε_F. Interestingly, when the normal metal is replaced by a ferromagnet, these bound states split, and for certain values of the exchange field, they cross the Fermi level [16]. As we shall show, this circumstance leads to a current flow. Clearly, the spontaneous current is strictly related to the zero energy states, as in the case of the high-T_c superconductors, but the origin of these states is completely different. As mentioned above, there are two competing parts to the total current in the $FFLO$ state. One is related to the unpaired electron movement and the other is a supercurrent. So one may expect, that in the case of the FM/SC heterostructure, these parts could be spatially unbalanced creating regions of net current flow. Indeed this is what we have discovered.

A brief report of our main results has already been published [23]. Here we wish to present a more detailed and systematic study of the zero energy Andreev bound states and the corresponding spontaneous current in the FM/SC heterostructures. The paper is organized as follows: in Section 2 the simple model which allows for self-consistent description of the FM/SC heterostructure is introduced. We also derive equations which have to be solved self-consistently. In particular, these include the Maxwell's equation (Ampere's law) for the coupling of the current to the magnetic field. Then we describe some technical details concerning the principal layer technique, which allows us to describe a semi-infinite superconductor. In Section 3 the nature of the Andreev bound states in the ferromagnet is discussed. The spontaneously generated current and corresponding magnetic field in the ground state are studied in the Section 4. In Section 5 we provide some suggestions of how one might observe the spontaneous current and its polarization experimentally. Finally, we conclude in Section 6.

2 The model

2.1 Negative U Hubbard model with exchange splitting

To study spontaneous currents and their polarization in the ferromagnet-superconductor heterostructure we have adopted a single orbital, nearest neighbour hopping Hubbard model with negative U on the SC side and zero U otherwise. Additionally we have assumed the site energies $\varepsilon_{i\sigma}$ to be exchange split in the ferromagnet and spin independent in the superconductor. Moreover, the simplest geometry allowing for a current flow is the $2D$ system, shown in Figure 1, where the magnetic field in one direction, the vector potential and the current in another and the spatial modulation in a third orthogonal direction are explicitly indicated. In short, our model Hamiltonian is given in the form:

$$H = \sum_{ij\sigma}[t_{ij} + (\varepsilon_{i\sigma} - \mu)\delta_{ij}]c^+_{i\sigma}c_{j\sigma} + \sum_{i\sigma}\frac{U_i}{2}\hat{n}_{i\sigma}\hat{n}_{i-\sigma} \quad (1)$$

where, in the presence of a vector potential $\mathbf{A}(\mathbf{r})$, the hopping integral is given by $t_{ij} = -t\mathrm{e}^{-\mathrm{i}\mathrm{e}\int_{\mathbf{r_i}}^{\mathbf{r_j}}\mathbf{A}(\mathbf{r})\cdot\mathrm{d}\mathbf{r}}$ for nearest neighbour lattice sites, whose positions are $\mathbf{r}_i$ and $\mathbf{r}_j$, and zero otherwise. The site energies $\varepsilon_{i\sigma}$ are 0 on the superconducting side and equal to $\frac{1}{2}E_{ex}\sigma$ on the ferromagnetic side, μ is the chemical potential, the on-site interaction U_i is $U_S < 0$ in the superconductor and zero elsewhere, $c^+_{i\sigma}$, $(c_{i\sigma})$ are the usual electron creation (annihilation) operators and $\hat{n}_{i\sigma} = c^+_{i\sigma}c_{i\sigma}$ is the electron number operator. Note that the above description of the electrons with charges e includes a coupling to a magnetic field $\mathbf{B}(\mathbf{r}) = \boldsymbol{\nabla}\times\mathbf{A}(\mathbf{r})$, which is necessary for calculating the effects of current on the electronic states. Furthermore, the exchange field is taken to be a bulk value and in these preliminary calculations we made no effort to be self-consistent with respect to the magnetization.

$$\hat{H}_{nm}(k_y) = \begin{pmatrix} \frac{1}{2}E_{ex}\delta_{nm} - T_- & -\Delta_n\delta_{nm} & 0 & 0 \\ -\Delta_n\delta_{nm} & \frac{1}{2}E_{ex}\delta_{nm} + T_+ & 0 & 0 \\ 0 & 0 & -\frac{1}{2}E_{ex}\delta_{nm} - T_- & \Delta_n\delta_{nm} \\ 0 & 0 & \Delta_n\delta_{nm} & -\frac{1}{2}E_{ex}\delta_{nm} + T_+ \end{pmatrix} \tag{3}$$

$$\hat{M}(\omega, k_y) = \begin{pmatrix} \hat{M}_{-N_F,-N_F} & \hat{M}_{-N_F,-N_F+1} & 0 & 0 & 0 & 0 & 0 & 0 & 0 \\ \hat{M}_{-N_F+1,-N_F} & \hat{M}_{-N_F+1,-N_F+1} & \hat{M}_{-N_F+1,-N_F+2} & 0 & 0 & 0 & 0 & 0 & 0 \\ 0 & \ddots & \ddots & \ddots & 0 & 0 & 0 & 0 & 0 \\ 0 & 0 & \hat{M}_{0,-1} & \hat{M}_{00} & \hat{M}_{01} & 0 & 0 & 0 & 0 \\ 0 & 0 & 0 & \hat{M}_{1,0} & \hat{M}_{1,1} & \hat{M}_{1,2} & 0 & 0 & 0 \\ 0 & 0 & 0 & 0 & \ddots & \ddots & \ddots & 0 & 0 \\ 0 & 0 & 0 & 0 & 0 & \hat{M}_{N_S,N_S-1} & \hat{M}_{N_S,N_S} & \hat{M}_{N_S,N_S+1} & 0 \\ 0 & 0 & 0 & 0 & 0 & 0 & \ddots & \ddots & \ddots \end{pmatrix}. \tag{4}$$

In what follows we shall work within the Spin-Polarized-Hartree-Fock-Gorkov ($SPHFG$) approximation, which means that we have approximated the interaction term in the Hamiltonian (1) by the usual mean field theory mapping: $\hat{n}_{i\uparrow}\hat{n}_{i\downarrow} \rightarrow \langle c_{i\downarrow}c_{i\uparrow}\rangle c^+_{i\uparrow}c^+_{i\downarrow} + \langle c^+_{i\uparrow}c^+_{i\downarrow}\rangle c_{i\downarrow}c_{i\uparrow}$. For the magnetic field we have chosen the Landau gauge where $\mathbf{B} = (0, 0, B_z(x))$ and hence $\mathbf{A} = (0, A_y(x), 0)$. Furthermore, we have assumed that the effective $SPHFG$ Hamiltonian is periodic in the direction parallel to the interface and therefore we work in $\mathbf{k}$ space in the y direction but in real space in the x-direction (see Fig. 1). Labelling the 'planes' (lines) in Figure 1 by integers n and m at each k_y point of the Brillouin zone we shall solve the following $SPHFG$ layer index (n) matrix equation for the retarded Green's function matrix $\hat{G}_{m'm}(\omega, k_y)$:

$$\sum_{m'k_y} \left(\omega\hat{\tau}_0\delta_{nm'} - \hat{H}_{nm'}(k_y)\right)\hat{G}_{m'm}(\omega, k_y) = \delta_{nm} \tag{2}$$

where $\hat{\tau}_0$ is the Pauli unit matrix and $\hat{H}_{nm}(k_y)$ is of the form:

see equation (3) above

with $T_\pm = (t\cos(k_y \pm eA_y(n)) + \mu)\delta_{nm} + t\delta_{n,n+1}$.

2.2 Semi-infinite superconductor

Our system consists of infinite number of layers (n), because we have a semi-infinite superconductor. The FM region spreads from $n = -N_F$ to 0, while the superconductor is defined for $n \geq 1$ (see Fig. 1). In order to describe the semi-infinite system, we need infinite range matrix with block elements $\hat{M}_{nm}(\omega, k_y) = \omega\hat{\tau}_0\delta_{nm} - \hat{H}_{nm}(k_y)$ (n, m going from $-N_F$ through 0 to ∞). In short, strictly speaking, we have to invert the infinite range matrix:

see equation (4) above

To render the problem traceable, it is useful to define the surface Green's function (SGF) [24] as

$$G^{sf}_{n,n}(\omega, k_y) = \{[\hat{M}_{n>N_S}(\omega, k_y)]^{-1}\}_{n,n} \tag{5}$$

$\hat{M}_{n>N_S}(\omega, k_y)$ being the semi-infinite submatrix for $n, m > N_S$ (lower right corner of the matrix in equation (4)). The physical meaning of the SGF is that it represents a square diagonal subblock corresponding to the semi-infinite bulk shown with a shaded region in Figure 1.

Now we can assume, that the electronic properties in the SC differ from that in the bulk only over the finite distance from the interface ($1 < n < N_S$). N_S can correspond to the distance of a few SC coherence lengths. For $n > N_S$ the electronic properties are that of the bulk superconductor. In other words, we assume that the system for $n > N_S$ is homogeneous. Namely, for $n > N_S$ we have:

$$\begin{aligned} \hat{M}_{n,n}(\omega, k_y) &= \hat{M}_{N_S,N_S}(\omega, k_y) \\ \hat{M}_{n,n+1}(\omega, k_y) &= \hat{M}_{N_S,N_S+1}(\omega, k_y) \\ \hat{M}_{n+1,n}(\omega, k_y) &= \hat{M}_{N_S+1,N_S}(\omega, k_y). \end{aligned} \tag{6}$$

As a consequence the surface Green's function (5) is also n-independent and can be obtained from the bulk GF [24]:

$$\begin{aligned} \hat{G}^{sf}(\omega, k_y) &= \hat{G}_{N_S,N_S}(\omega, k_y) \\ &\times (1 + \hat{M}_{N_S+1,N_S}(\omega, k_y)\hat{G}_{N_S,N_S+1}(\omega, k_y))^{-1} \end{aligned} \tag{7}$$

where $\hat{G}_{n,m}(\omega, k_y)$ is the Fourier transform of the Green's function of the homogeneous superconductor $\hat{G}(\omega, k_x, k_y)$, namely $\hat{G}_{n,m}(\omega, k_y) = \frac{1}{N_{kx}}\sum_{k_x}\hat{G}(\omega, k_x, k_y)\mathrm{e}^{-\mathrm{i}k_x(R_n - R_m)}$. Clearly, the Green's function $\hat{G}(\omega, k_x, k_y)$ for the case where the vector

$$\hat{M}(\omega,k_y)=\begin{pmatrix} \hat{M}_{-N_F,-N_F} & \hat{M}_{-N_F,-N_F+1} & 0 & 0 & 0 & 0 & 0 \\ \hat{M}_{-N_F+1,-N_F} & \hat{M}_{-N_F+1,-N_F+1} & \hat{M}_{-N_F+1,-N_F+2} & 0 & 0 & 0 & 0 \\ 0 & \ddots & \ddots & \ddots & 0 & 0 & 0 \\ 0 & 0 & \hat{M}_{0,-1} & \hat{M}_{00} & \hat{M}_{01} & 0 & 0 \\ 0 & 0 & 0 & \hat{M}_{1,0} & \hat{M}_{1,1} & \hat{M}_{1,2} & 0 \\ 0 & 0 & 0 & 0 & \ddots & \ddots & \ddots \\ 0 & 0 & 0 & 0 & 0 & \hat{M}_{N_S,N_S-1} & \hat{M}_{N_S,N_S}-\hat{\Gamma}_{N_S} \end{pmatrix}. \quad (9)$$

potential is equal to zero is given by the usual result:

$$\hat{G}(\omega,k_x,k_y)=\frac{1}{\omega^2-(\xi_{\mathbf{k}}^2+\Delta^2)} \times\begin{pmatrix} \omega+\xi_{\mathbf{k}} & -\Delta & 0 & 0 \\ -\Delta & \omega-\xi_{\mathbf{k}} & 0 & 0 \\ 0 & 0 & \omega+\xi_{\mathbf{k}} & \Delta \\ 0 & 0 & \Delta & \omega-\xi_{\mathbf{k}} \end{pmatrix} \quad (8)$$

where $\xi_{\mathbf{k}}=-2t(\cos(k_x)+\cos(k_y))-\mu$ is the single electron energy spectrum.

The homogeneity of the system for $n > N_S$ leads to the conclusion, that the inversion of a semi-infinite block tridiagonal matrix (4) can be reduced to the inversion of the finite tridiagonal matrix:

see equation (9) above

In the above equation the effect of the semi-infinite homogeneous system is contained in the 'embedding potential' $\hat{\Gamma}_{N_S}$, which is related to the surface Green's function through:

$$\hat{\Gamma}_{N_S}(\omega,k_y)=\hat{M}_{N_S,N_S+1}(\omega,k_y) \times\hat{G}^{sf}(\omega,k_y)\hat{M}_{N_S+1,N_S}(\omega,k_y). \quad (10)$$

Evidently, by increasing N_S until $\hat{G}_{nm}(\omega,k_y)$ in the surface region does not change would constitute an exact albeit numerical solution of the equation (2). All calculations reported here were performed for $N_S = 20$. However, we have checked that larger N_S has no influence on the results.

2.3 Finite temperature method

The calculation of the various physical quantities, like particle concentration n_n, spin polarization m_n, order parameter Δ_n, etc., needs the evaluation of integrals of the product of the Green's function and Fermi distribution function as in $\int \mathrm{d}\omega G(\omega)f(\omega)$. While working on the real energy axis, we need a large number of integration points to get good accuracy, unless there are no singularities in the density of states. However, in our calculations, there is a Van Hove singularity in the $2D$ DOS as well as BCS-like singularities. In fact we need approximately 10^3–10^4 points to get good accuracy, which is very time-consuming in self-consistent calculations. The situation is similar for summation over the Matsubara energies $\omega_\nu=(2\nu+1)\pi\mathrm{i}/\beta$ because of the poles of the Fermi function. There is an infinite number of poles, and this infinite sum does not always converge well, so numerical treatment needs a large number of data points.

To overcome these difficulties we follow reference [25] and approximate the Fermi distribution function by:

$$f^c(\omega)=\frac{1}{\left(\frac{\omega+\sigma}{\sigma}\right)^{2N}+1}. \quad (11)$$

To get the correct behaviour near the Fermi energy ($E_F = 0$) we choose $2N=\beta\sigma$. One can check, that the discrepancy between the approximate function and the true one, starts to play role for energies lower than 2σ. If we choose $2\sigma > W$, where $W = 2t$ is the half of the bandwidth, the approximation works very well. For example, for the temperature $T = 10^{-2}t$ it is sufficient to consider only 150 points to get very good accuracy.

The poles of the approximate function lie on a circle given by

$$\left(\frac{\omega+\sigma}{\sigma}\right)^{2N}+1=0. \quad (12)$$

The solution of the above equation gives the poles in the form:

$$\omega=-\sigma+\sigma\mathrm{e}^{(2\nu+1)\pi i/2N}. \quad (13)$$

In the limit $\sigma\to\infty$, the poles (13) move to the Matsubara energies, and the number of poles, $2N$, becomes infinite.

The calculation of any physical quantity becomes:

$$\langle\hat{O}\rangle=\frac{2}{\pi}\sum_{\nu=0}^{2N-1}\mathrm{Re}G(\omega_\nu)\mathrm{e}^{(2\nu+1)\pi\mathrm{i}/2N} \quad (14)$$

where ω_ν is given by equation (13).

2.4 Self-consistency with the Ampere's law

As usual in problems of interfaces, a large number of equations has to be solved self-consistently. In our case the parameters, to be determined self-consistently at each layer n, are: the total electron density n_n, the spin polarization m_n, the SC order parameter Δ_n, the current parallel to the interface $J_y(n)$ and the vector potential $A_y(n)$.

Most of these quantities can be expressed in terms of the corresponding layer-diagonal elements of the Green's functions $\hat{G}_{nn}(\omega, k_y)$ (see Eq. (3)). The exception is the vector potential, for which we need an additional (Maxwell's) equation. These relations are (see Eq. (14)):

$$n_n = n_{n\uparrow} + n_{n\downarrow} = \frac{2}{\beta}\sum_{ky}\sum_{\nu=0}^{2N-1} \times \mathrm{Re}\left\{(G^{11}_{nn}(\omega_\nu, k_y) + G^{33}_{nn}(\omega_\nu, k_y))\mathrm{e}^{(2\nu+1)\pi\mathrm{i}/2N}\right\} \tag{15}$$

$$m_n = n_{n\uparrow} - n_{n\downarrow} = \frac{2}{\beta}\sum_{ky}\sum_{\nu=0}^{2N-1} \times \times \mathrm{Re}\left\{(G^{11}_{nn}(\omega_\nu, k_y) - G^{33}_{nn}(\omega_\nu, k_y))\mathrm{e}^{(2\nu+1)\pi\mathrm{i}/2N}\right\} \tag{16}$$

$$\Delta_n = U_n \sum_{k_y}\langle c_{n\downarrow}(k_y)c_{n\uparrow}(k_y)\rangle = \frac{2U_n}{\beta}\sum_{ky}\sum_{\nu=0}^{2N-1}\mathrm{Re}\left\{G^{12}_{nn}(\omega_\nu, k_y)\mathrm{e}^{(2\nu+1)\pi\mathrm{i}/2N}\right\} \tag{17}$$

where $G^{ij}_{nn}(\omega, k_y)$ is the ijth element of the matrix Green's function, which is the solution of the $SPHFG$ equation (Eq. (2)).

The current, for spin up electrons, in the y-direction can be calculated from the relation:

$$J_{y\uparrow(\downarrow)}(n) = \frac{4et}{\beta}\sum_{k_y}\sin(k_y - eA_y(n)) \times \sum_{\nu=0}^{2N-1}\mathrm{Re}\left\{G^{11(33)}_{nn}(\omega_\nu, k_y)\mathrm{e}^{(2\nu+1)\pi\mathrm{i}/2N}\right\} \tag{18}$$

which follows from the continuity equation for the charge ($e\frac{\mathrm{d}n_i}{\mathrm{d}t} = -e[n_i, H]_- = -\sum_j J_{ij}$).

This current will give rise to a vector potential $A_{new}(\mathbf{r})$ which will have to be used to update $A(\mathbf{r})$ in equation (2) at the end of each self-consistency cycle. We calculated this new vector potential by solving numerically Ampere's law, $\frac{\mathrm{d}^2A_y(x)}{\mathrm{d}x^2} = -4\pi J_y(x)$, which for the lattice problem at hand, is

$$A_y(n+1) - 2A_y(n) + A_y(n-1) = -4\pi J_y(n). \tag{19}$$

In all our calculations equations (15–19) have been solved in each iteration step until self-consistency has been achieved. The numerical calculations have been performed at temperature $T = 10^{-2}t$ for 150 energy points, 120-k_y points and 40 layers (20 ferromagnetic and 20 superconducting). Typically self-consistency, at the level of 0.01 % on all densities in equations (15–19), has been achieved after 100–200 iterations.

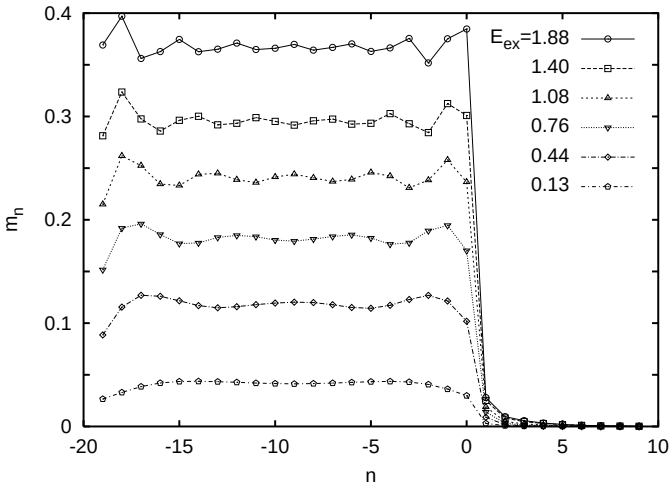

Fig. 2. Magnetization as a function of the distance from the interface for a number of exchange fields (E_{ex}) and $U_S = -2$, which gives $\Delta_S = 0.376$ in units of the hopping integral t.

3 Andreev bound states in ferromagnet

3.1 Superconducting and ferromagnetic order parameters

Since we have determined the ferromagnetic (16) and superconducting (17) order parameters on both sides of the interface fully self-consistently, we were able to study both SC and FM proximity effects. This means, that we were able to describe situations in which ferromagnetism and superconductivity coexist near the interface.

Firstly, we want to discuss the magnetic proximity effect, namely the entering of the spin polarization into the superconductor. The typical behaviour of the spin polarization ($m_n = n_{n\uparrow} - n_{n\downarrow}$) is plotted in the Figure 2 as a function of the layer index n for a number of exchange splittings E_{ex}. Note that m_n calculated is the response to the bulk value of the exchange splitting, which has not been updated at the end of each self-consistency cycle. A similar procedure was used by Zhu and Ting [26] with very similar results to those we have obtained. Returning to the results we can see that the spin polarization exponentially decays over the distance of the SC coherence lengths ξ_S, which in the present case is $\xi_S \approx 3$ in units of the lattice constant a. We have checked this by explicit calculations of ξ_S for various values of the superconducting energy gap. So we can conclude that effect of proximity of the ferromagnet on the superconductor is very similar to case of the Meissner effect, where an external magnetic field is excluded from the sample. Note however that while the magnetic field is excluded on the spatial scale of the penetration depth the effective exchange field drops to zero within the distance of the coherence length ξ_S in the superconductor. Similar behavior of the induced exchange splitting in SC was obtained by Tokuyasu *et al.* [27].

More interesting is the behaviour of the spin polarization on the ferromagnetic side of the heterostructure. As it is seen from Figure 2, it oscillates around its bulk value with period depending on the exchange splitting E_{ex}

but not on the superconducting gap. However we were not able to fit the numerical points to any simple relation between parameters of the model. The best fit we have is $m_n \propto \sin((1.74E_{ex}+0.5)n)$. Whilst this means that the period of the oscillations is a linear function of the exchange splitting the above relation is valid only for the thickness of the FM slab $d = 20$ layers. For different thicknesses we have different relations and different numbers of period within the slab. For example, for $d = 10$, m_n shows one period less for the corresponding exchange splittings E_{ex}.

We now turn to the superconducting proximity effect, namely the leakage of the SC properties into the non-superconducting region. In our case, although $\Delta_n = 0$ on the ferromagnetic side, due to the fact that for $n \leq 0$, $U_n = 0$, the pairing amplitude $\chi_n = \langle c_{n\downarrow} c_{n\uparrow} \rangle$ can, in general, be non-zero and it usually is.

The proximity effect is well understood in the case of non-magnetic metal-superconductor interface (NM/SC) [5] in terms of the Andreev reflections [6]. The Andreev process describes a situation in which an electron impinging onto the NM/SC interface is reflected back as a hole (with opposite spin) and a Cooper pair is created in the SC. Moreover, the movement of the electrons and holes in the NM close to the interface (over the distance of the SC coherence length ξ_S) is highly correlated. The pairing amplitude, in this case, enters the normal metal and decays exponentially over the ξ_S.

When the normal metal is replaced by a ferromagnet one might naively expect that the proximity effect will be suppressed due to the pair breaking effect of the exchange field [28] . This suggests that the pairing amplitude χ_n will decay over a distance much shorter than the superconducting coherence length. Remarkably, as we can see in Figure 3, this is not the case. Instead, we can observe a very long range proximity effect with an oscillating pairing amplitude. This effect has been first noted by Buzdin *et al.* [10,11] and have been studied in several recent publications [12,13,16,26,29–31]. According to them, it can be attributed to a $FFLO$-like phenomena [8,9] in FM/SC heterostructures. The period of the oscillations of the χ_n depends on the exchange splitting E_{ex} (see Fig. 3) and, similarly to the oscillations of m_n, does not depend on the superconducting energy gap. Clearly this behaviour is different from NM/SC case, where the proximity effect depends on the SC coherence length ξ_S. Here, it depends only on the properties of the ferromagnet. Moreover, the numerically obtained behaviour of the pairing amplitude χ_n is consistent with the analytical formula

$$\chi_n \propto \sin(n/\xi_F)/(n/\xi_F) \tag{20}$$

with $\xi_F = 2t/E_{ex}$ being ferromagnetic coherence length. Reassuringly this result is fully consistent with those of references [13,16,26,29–31]. The comparison our numerical results with the formula (20) for the exchange splitting $E_{ex} = 1.88$, which gives $\xi_F = 1.06$ is depicted in the inset of the Figure 3. In fact we had to change ξ_F by 5%, in order to get better fit. So the solid line in the inset of the Figure 3 corresponds to the formula

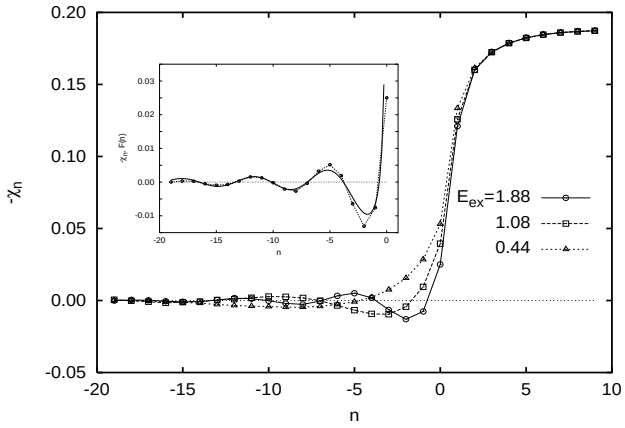

Fig. 3. The pairing amplitude $-\chi_n$ *vs.* layer index n for three values of the exchange field E_{ex}. Note that we plot $-\chi_n$ which corresponds to positive Δ_n for $U_n > 0$. Inset: Comparison of the numerical results with the analytical formula $\chi_n \propto \sin(n/\xi_F)/(n/\xi_F)$ for the exchange field $E_{ex} = 1.88$, which gives $\xi_F = 1.06$. In fact we had to change ξ_F by 5% in order to get better agreement. The solid line is our fit: $\chi_n = 0.021 \sin(n/\tilde{\xi}_F - 2.5)/(n/\tilde{\xi}_F)$, where $\tilde{\xi}_F = \xi_F/1.05$.

$\chi_n = 0.021 \sin(n/\tilde{\xi}_F - 2.5)/(n/\tilde{\xi}_F)$ with $\tilde{\xi}_F = \xi_F/1.05$. It turns out that as exchange splitting becomes smaller the fitting to the analytical formula (20) becomes better. The small discrepancy in the coherence length may come from the fact, that we have used bulk value of the exchange field while calculating the coherence length. However in our system, the spin polarization oscillates around its bulk value, and if we calculate the average value of the spin polarization $\bar{m} = \frac{1}{N_F+1} \sum_{n \leq 0} m_n$, we get a little bit smaller value than the bulk one. So, we conclude, that the effective exchange splitting $\tilde{E}_{ex}$ also has to be smaller than its bulk value. Indeed, when we used $\tilde{E}_{ex}$ to calculate the coherence length, the agreement is improved. Another reason may be the approximate form of the formula for the coherence length in the lattice case $\xi_F \approx 2t/E_{ex}$. In any case these difficulties imply that the calculations would need to be self-consistent with respect to m_n as well as χ_n and j_n.

3.2 Density of states and the Andreev levels

The proximity effect manifests itself not only in the pairing amplitude and the spin polarization characteristics but also in the density of states (DOS). The layer resolved DOS is defined as

$$\rho_n(\omega) = \rho_{n\uparrow}(\omega) + \rho_{n\downarrow}(\omega) = -\frac{1}{\pi} \sum_{k_y} \mathrm{Im}(G^{11}_{nn}(\omega + \mathrm{i}0^+, k_y) + G^{33}_{nn}(\omega + \mathrm{i}0^+, k_y)) \tag{21}$$

with $G^{ij}_{nn}(\omega + \mathrm{i}0^+, k_y)$ being the ijth element of the matrix Green's function-solution of equation (2). We shall also use the density of states integrated over the total sample: $\rho_{tot}(\omega) = \sum_n \rho_n(\omega)$.

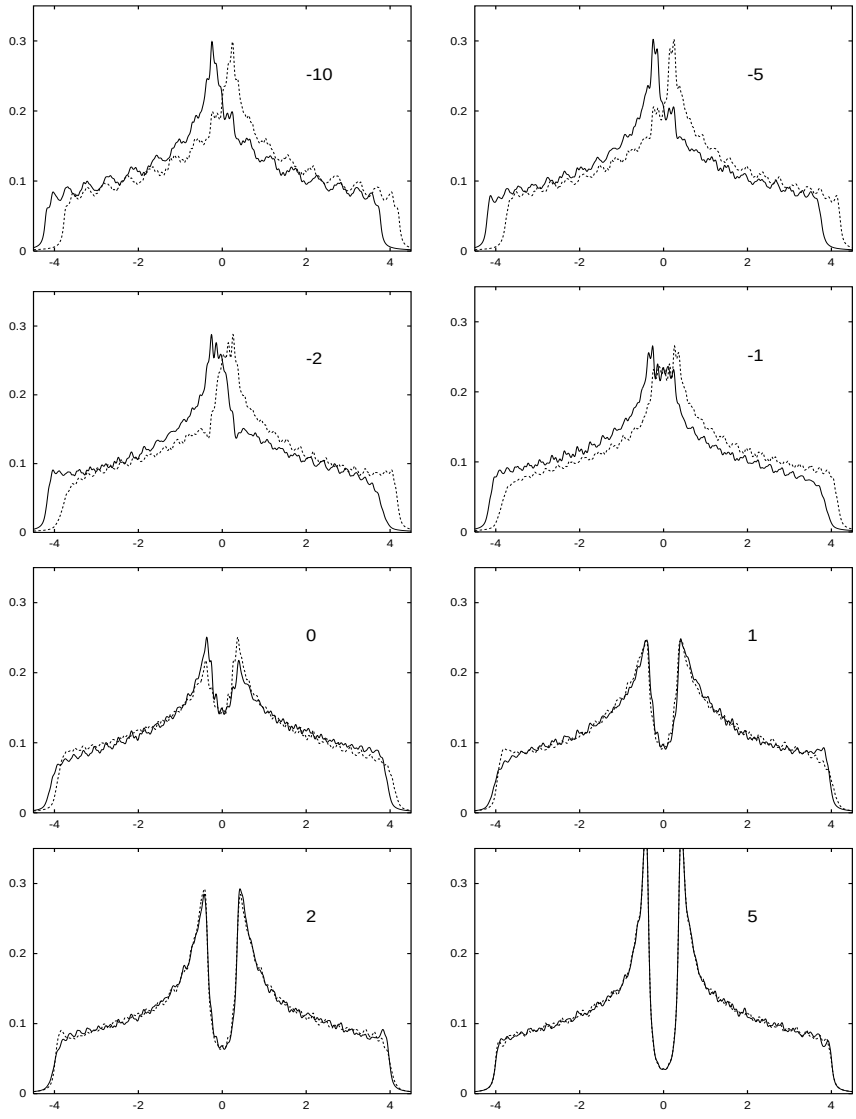

Fig. 4. The layer resolved density of states for the spin up (solid line) and spin down (dashed line) electrons for the exchange splitting $E_{ex} = 0.44$. The layer index is shown in the panels.

At this point we want to stress that, when we calculate thermodynamic quantities (Eqs. (15–18)) we work on the complex energy plane, but calculating the *DOS* we solve equation (2) on the real energy axis only once. In fact we have added a small imaginary part ($0^+ = 0.005$) for numerical purposes. The quantities: n_n, m_n, Δ_n, $A_y(n)$ as determined by the previous self-consistent procedure allow us to find the Green function on the real energy axis in only one step. We also check if the new quantities like n_n, m_n, etc. agree with the old ones. For all such calculations the agreement has been found to be excellent.

While the general solution of equation (2) allows for a current flow, in this section we show the results for a solution for which the current has been constrained to be zero.

To appreciate the effect of spin polarization in the FM slab, let us recall again the case of no exchange splitting. If the non-magnetic metal (NM) is in the contact with superconductor (SC), the density of states on the NM side shows features of the *SC DOS*, *i.e.* the pseudo-gap opens up around the Fermi energy in the *DOS*. However it never turns into a true gap, namely the *NM DOS* always possess low energy excitations. Moreover, the gap in the *SC DOS* also starts to fill up, due to the proximity of the normal metal. So in this case we deal with gapless superconductivity close to the interface of the NM/SC heterostructure.

Compared to the above summary, the ferromagnet-superconductor interface is enriched with a number of new features. For instance, the *SC DOS* splits, if the exchange field is small. For strong enough exchange field, SC gap can be suppressed, indicating transition to the non-SC (normal) phase. An example of the layer resolved density of states for spin up (solid line) and down (dashed) is shown in Figure 4. Evidently there is a pseudogap in the *FM DOS*, indicating that superconducting correlations are present in the FM layers. This effect is particularly strong for the layer index $n = 0$ and -1. On the other

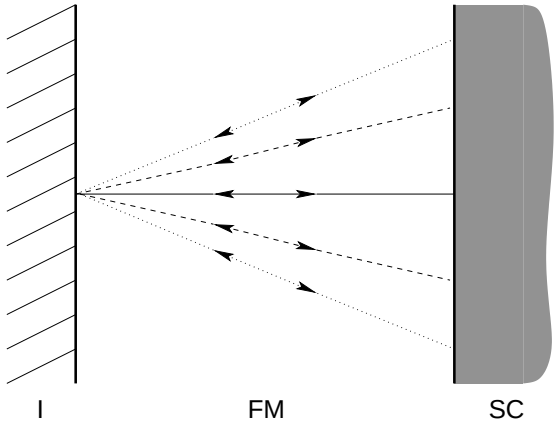

Fig. 5. Schematic view of the semi-classical paths of impinging electrons and reflected holes corresponding to the different Andreev bound states.

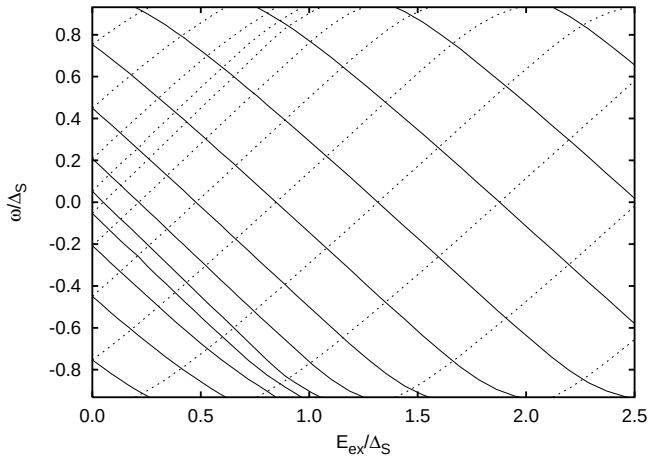

Fig. 6. The position of the Andreev bound states *vs.* exchange splitting E_{ex} for the 20 layers thick ferromagnet. The solid (dashed) line corresponds to the spin up (down) electrons. Note that energy is now measured in units of the bulk superconductor order parameter Δ_S. The basic physics represented by this plot is the same as the ω/Δ_S *vs.* d (thickness of the FM sample) curves of reference [16].

hand, the proximity of the ferromagnet leads to the existence of low energy states in the SC DOS. This effect is also observed in NM/SC heterostructure but here we also notice differences in the spin up and spin down DOS on the SC layers close to the interface. These are clear manifestations of the FM proximity effect. The density of states (its polarization) on SC side is very similar to the density of states of a superconductor in an external magnetic field [32].

The most interesting physics of the heterostructures we consider, is the formation of Andreev bound states in the NM or FM layers. They are 'particle in a box' like states which can be associated with the semiclassical orbits bouncing back and forth between the SC and I regions, as depicted in Figure 5. As is well known in the case of NM layers the reflections at the SC are Andreev ones, while those at the I are normal reflections [22]. The arrows in Figure 5 point along the momenta of the particle segment of the orbit. Its y component is k_y which labels the state. Clearly, the collection of states labelled in this way forms an Andreev band.

For the normal metal-superconductor heterostructure, Andreev bound states (bands) are symmetrically placed with respect to the Fermi energy. Of course the position of these states changes with the thickness of the sample. As we increase the size of the sample, the Andreev bound states approach the Fermi energy, but they will never reach it. In other words, there is no possibility of crossing the Fermi level. Somewhat surprisingly, the situation is quite different for the FM/SC structure [16]. In this case the bound state energies can cross the Fermi level. In short they can become the zero-energy mid-gap states [21]. This situation is illustrated, for $k_y = 0$, in Figure 6, where the bound state energies are plotted against the exchange splitting.

If we take into account states for different k_y (Andreev band), the situation is more complicated as in general the states with different symmetry of the wave function can mix, and so we are not able to separate Andreev bands so easily. The example of such Andreev bands rather than

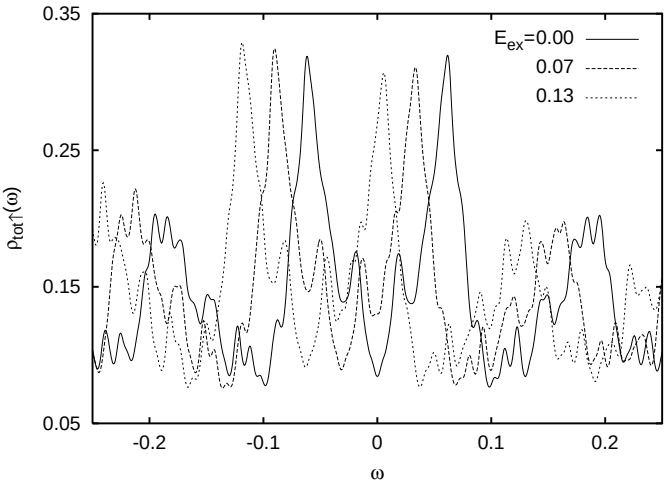

Fig. 7. The total density of states ($\rho_{tot\uparrow}(\omega) = \sum_n \rho_{n\uparrow}(\omega)$) of the spin up electrons for various values of the exchange splitting E_{ex} indicated on the picture. Note the shift of the Andreev bound states (bands) with exchange splitting. The DOS for spin down electrons can be easily obtained by reflection of the spin up electrons DOS with respect to the Fermi energy $\varepsilon_F = 0$.

states is shown in Figure 7, where the density of states of the spin up electrons is plotted for a few values of the exchange splitting.

As we shall report presently the fact that the Andreev bound states can cross the Fermi level has remarkable consequences: it leads to the generation of the spontaneous current in the ground state.

In fact the situation is rather similar to that of exotic superconductors (with non-s-wave order parameter), where the surface DOS shows the zero-energy state, leading to the spontaneously generated current. However the

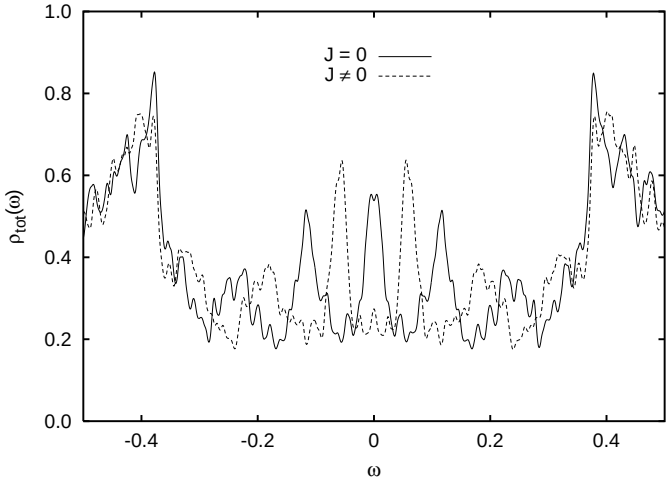

Fig. 8. The Doppler splitting of the zero energy state in the density of states $\rho_{tot}(\omega) = \sum_n (\rho_{n\uparrow}(\omega) + \rho_{n\downarrow}(\omega))$ caused by the spontaneous current for $E_{ex} = 0.13$. The solid (dashed) line corresponds to the solution without (with) the current in the ground state.

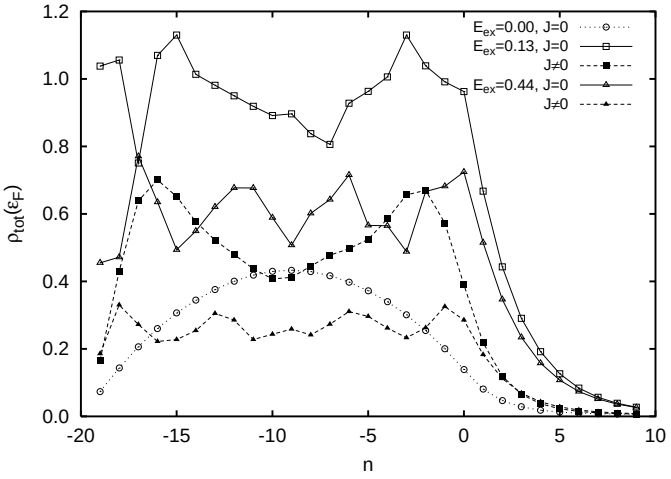

Fig. 9. The layer resolved density of states at the Fermi energy $\varepsilon_F = 0$ for different exchange splittings. The filled (empty) symbols correspond to the solution with (without) the current.

origin of this state is quite different, as there it comes from the symmetry related sign change of the order parameter at the surface [21]. Here, in the FM/SC heterostructure, the zero-energy state comes from the oscillatory behaviour of the pairing amplitude (χ) in FM, which changes its phase by π each time crosses zero. Nevertheless it leads to the same effect: a spontaneously generated current.

4 Current in the ground state

4.1 Splitting of the zero energy state

The most remarkable feature of our calculations is that the solution of the $SPHFG$ equations frequently converges to a solution with the finite current $j_y(n)$ even though the external vector potential is zero. The generation of the spontaneous current is strictly related to the crossing of the Andreev bound states through the Fermi energy. In Figure 7, we have plotted the DOS for different values of the exchange splitting for calculations where the current was allowed to develop in the y-direction. For the $E_{ex} = 0.13$ we observe that spontaneous current is generated in the ground state. We have checked that the solution with the current flowing is the true ground state, as it has energy lower than solution without the current. Physically, in the presence of the current, the zero energy states split because of the momentum dependence of a $\mathbf{p} \cdot \mathbf{v}$ contribution to the quasiparticle energies where the velocity vector is defined by the current $\mathbf{J} = en\mathbf{v}$. The example of such a Doppler splitting in the DOS is shown in Figure 8 for the exchange field $E_{ex} = 0.13$. We can see that, besides the zero energy state, the other Andreev states also are split. It turns out that the splitting of these states is only weakly sensitive to the exchange field E_{ex}, but it strongly depends on the thickness of the ferromagnetic slab and it decreases as the thickness increases.

Interestingly, we have found a simple relation between the splitting of the zero energy state δ and the vector potential $A_y(n)$. This is given by:

$$\delta \approx 2et\bar{A}_y \tag{22}$$

where $\bar{A}_y$ is the value of the vector potential $A_y(n)$ averaged over the FM side of the system only, *i.e.* $\bar{A}_y = \frac{1}{N_F+1} \sum_{n \leq 0} A_y(n)$.

Corresponding to the splitting of the zero energy states, when the current flows, we find differences in the DOS at the Fermi level. In fact, the difference is quite small. The main behaviour remains the same. The comparison of the density of states at the Fermi energy for both cases ($J = 0$ and $J \neq 0$) is shown in Figure 9. The DOS for the NM/SC structure (dashed line with circles) is also drawn. As we can see, the main features remain more or less the same, in particular the period of the oscillations. Similarly like the spin polarization (Fig. 2) and pairing amplitude (Fig. 3), the density of states at the Fermi level shows decreasing period of the oscillations as the exchange splitting increases.

4.2 Spontaneous current and the magnetic flux

As we already discussed, the zero energy state is responsible for the generation of the spontaneous current in the system. The typical example of such a current, flowing parallel to the FM/SC interface, ($j_y^{tot}(n) = j_{y\uparrow}(n) + j_{y\downarrow}(n)$) is shown in Figure 10 for a few values of the exchange splitting. Evidently, the behaviour of the current, as a function of the layer index, is very similar to the density of states at the Fermi level. For example, if we compare the dashed curve with the triangles in Figure 10 to the dashed or solid

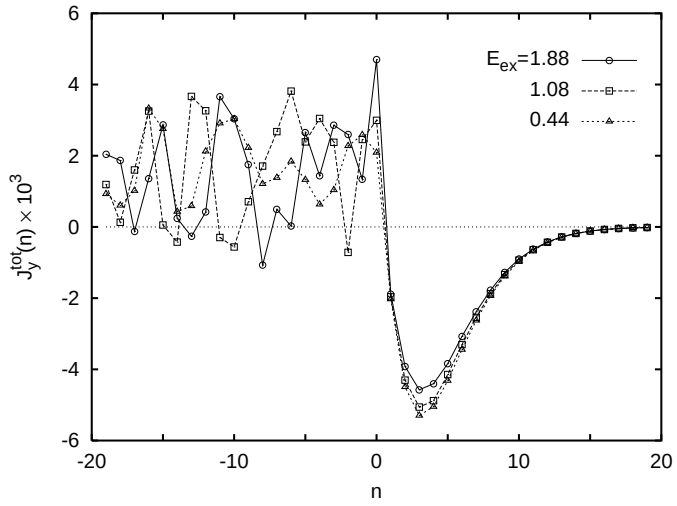

Fig. 10. The total (spontaneous) current $j_y^{tot}(n) = j_{y\uparrow}(n) + j_{y\downarrow}(n)$ flowing parallel to the FM/SC interface for a number of exchange splittings.

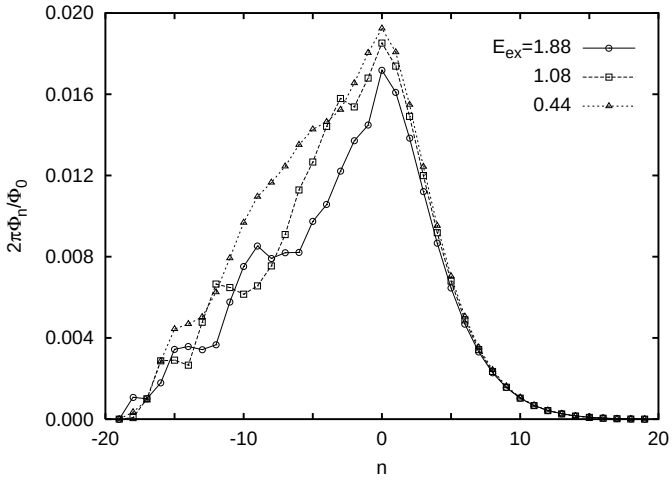

Fig. 11. The (spontaneous) magnetic flux per plaquette associated with layer n and $n+1$ for a number of exchange splittings. Each curve corresponds to the related current shown in Figure 10. $\Phi_0 = h/2e$ is the flux quantum and a is the lattice constant in units of Å.

line with triangles in Figure 9, we readily notice the similarity in the oscillating nature of the current and DOS respectively.

Another important issue is the distribution of the current through the whole trilayer structure. We find that it flows mostly in the positive y direction on ferromagnetic side and in the negative direction in the superconductor. Notably the total current, integrated over the whole sample, is equal to zero within numerical accuracy. This is as it should be for the true ground state and found to be in the $FFLO$ state, where the current associated with the unpaired electrons is balanced by the supercurrent flowing in the opposite direction.

While the total current in the system is equal to zero, the current integrated over FM side only ($J_{FM}^{tot} = \sum_{n\leq 0} J_y^{tot}(n)$) has a finite value, almost independent of the exchange splitting. But that current is very sensitive to the thickness of the FM slab, and for example for $N_F = 10$ $J_{FM}^{tot} \approx 0.08\ e\hbar t$ (0.008 per layer), while for $N_F = 20$ we have $J_{FM}^{tot} \approx 0.035\ e\hbar t$ (0.00175 per layer). This suggests that the effect associated with the spontaneous current is very important in the samples of the small thicknesses and it seems to play minor role if the size of FM part of the system is large.

Obviously, the above current distribution should lead to the generation of the magnetic flux through the sample. In fact we have found that again, as for the current, the magnetic flux bounded by the layers only weakly depends on the exchange splitting but it does change with the distance from the interface. For $N_F = 10$ the magnetic flux $\Phi^{tot} = \sum_{n\leq 0} \Phi_n \approx 0.45\Phi_0$, where $\Phi_0 = h/2e$ is the flux quantum. This gives a flux per plaquette, associated with the layers n and $n+1$, $\Phi_n \approx 0.045\Phi_0$. On the other hand, for $N_F = 20$ we have $\Phi^{tot} \approx 0.25\Phi_0$ and $\Phi_n \approx 0.0125\Phi_0$ respectively.

The typical layer dependence of the spontaneous magnetic flux Φ_n (magnetic flux through a plaquette) is shown in Figure 11. We can see that while there are small differences in the behaviour on the FM and SC sides of the sample, related to the different current distributions (see Fig. 10), the total magnetic flux Φ^{tot} is roughly the same and more or less independent of the exchange splitting.

4.3 Quasiparticle current vs. supercurrent

As we have recalled above, in the bulk $FFLO$ state the total current vanishes. Moreover, the quasiparticle current J^{qp} is exactly equal to the supercurrent J^{sc} (related to the $G_{nn}^{12}(\omega, k_y)$ in Eq. (2)) with opposite sign. This means that in a bulk layered superconductor, these two currents cancel each other layer by layer, *i.e.* $J^{qp}(n) = -J^{sc}(n)$. Evidently this is the case because the exchange field and superconducting pairing potential are present in the whole system. By contrast, in the case of the FM/SC heterostructure, the exchange field and the pairing potential are spatially separated. In this case $J^{qp}(n)$ is not equal to $-J^{sc}(n)$ within each layer, but it is when integrated over the whole sample, *i.e.*

$$\sum_n J^{qp}(n) = -\sum_n J^{sc}(n). \tag{23}$$

Thus the lack of exact cancellation of the current layer by layer leads to a finite current on both sides of the interface, but zero in the whole sample. An example of such behaviour is shown in Figure 12. We see, that the quasiparticle part of the total current (solid line) is almost in anti-phase to the supercurrent (dashed line). Moreover, on the superconducting side, the current is carried mainly by quasiparticles. This is rather surprising since usually one expects current to be related to the Cooper pairs. However due to the proximity of the ferromagnet, there are also

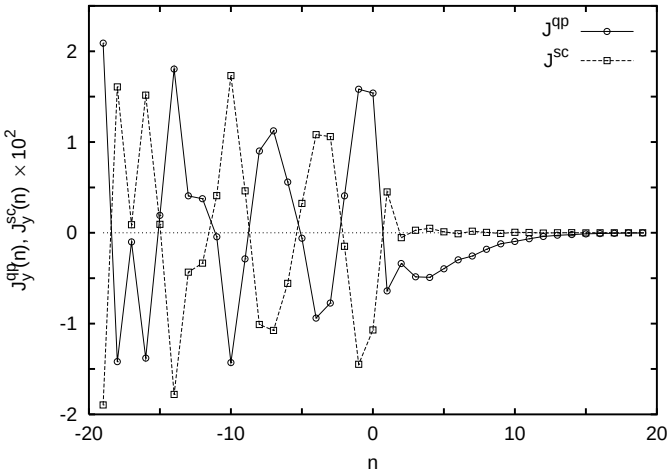

Fig. 12. Layered resolved quasiparticle current (solid line) and supercurrent (dashed line) for exchange splitting $E_{ex} = 1.88$. This corresponds to the total current (solid line with circles) shown in Figure 10.

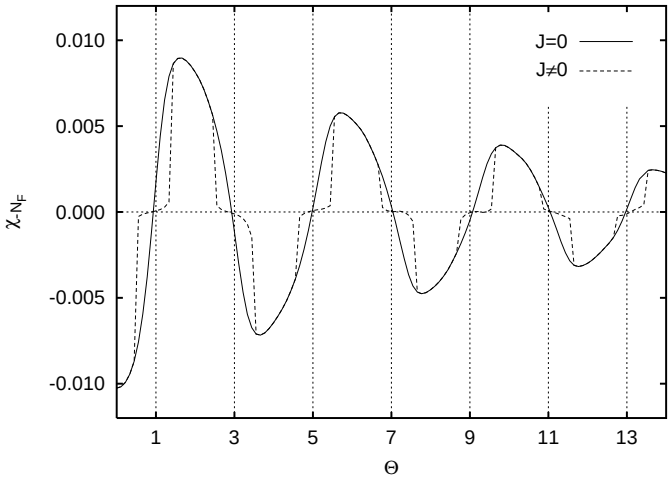

Fig. 13. Pairing amplitude at the FM surface opposite to superconductor ($n = -N_F$) as a function of the dimensionless parameter $\Theta = 2.79 dE_{ex}/\pi t$.

'normal' particles in the superconductor near the interface. These certainly contribute to the total current, like in the bulk $FFLO$ state. In our system, only the Cooper pairs close to the interface can feel the exchange field of the ferromagnet and have moving center of mass. Note that magnetization goes to zero very quickly as we go away from the interface (see Fig. 2). Clearly this makes the supercurrent equal to zero except within a few SC layers.

Interestingly we also found that whenever the pairing amplitude χ_n changes sign, the local quasiparticle current as well as the local supercurrent becomes large. In other words, the maxima of the $J^{qp}(n)$ and $J^{sc}(n)$ correspond to the zeros of the pairing amplitude χ_n.

4.4 The pairing amplitude at I/FM interface

As we have mentioned above, the ground state does not carry current for all values of the exchange splitting. We have shown, that whenever there is a current flowing, there are the Andreev bound states crossing the Fermi level. Also we have found another quantity which is related to the current flowing. Namely, the pairing amplitude at the FM/I interface (*i.e.* $n = -N_F$ – see Fig. 1). If χ_{-N_F} changes its sign, the spontaneous current is generated. This happens exactly for the same values of the exchange splitting, for which a band of the Andreev bound states crosses the Fermi energy. Moreover, the presence or absence of the current has a dramatic effect on the pairing amplitude χ_{-N_F}. This can be seen in Figure 13, where χ_{-N_F} is plotted as a function of the dimensionless parameter $\Theta = 2.79 dE_{ex}/\pi t$. As implied by equation (17), χ_n is the real part of a complex order parameter which has an amplitude $\bar{\chi}_n$ and a phase $\bar{\varphi}_n$. Clearly, Figure 13 can be read as $\bar{\varphi}_{-N_F}$ flipping from $\varphi^0_{-N_F}$ where χ_{-N_F} has the same sign as χ in SC, to $\varphi_{-N_F} = \pi$, where χ_{-N_F} has the opposite sign.

Evidently, the pairing amplitude is pinned to zero by the spontaneous current in the system. Introducing the dimensionless quantity Θ we can say, that system is in a π-like phase (for odd Θ) or in the 0-phase (even Θ), in close analogy to studies on the π-effect in the $SC/FM/SC$ structure by Chtchelkatchev *et al.* [33]. In reference [23], we have shown a similar picture for the thickness of the FM slab equal to 10 layers. Here we show the corresponding results for $N_F = 20$ layers. To be precise in the present case Θ has slightly different value with prefactor 2.79 (not 3 as it was for 10 layers case). This discrepancy may come from the fact, that effective exchange splitting is little bit smaller than its bulk value (see discussion in Sect. 3.1).

4.5 Band filling and the polarization of the current

As our system consists of a ferromagnet and a superconductor, we can expect the spontaneous current to be polarized. However, up to now, we have presented results for the special case of particle-hole symmetry ($n_e = 1$ or $\mu = 0$) and we found that the spontaneous current was, in fact, not spin-polarized. The reason is as follows. Within linear response theory, the total current can be divided into two parts: a diamagnetic one – giving the response of the bulk density, and a paramagnetic one, which is proportional to the density of states at the Fermi energy, as it comes from the deformation of the wave function at the Fermi surface [34]. Now if we note, that for the particle-hole symmetric case ($n_e = 1$), the spin up $\rho_{tot\uparrow}(\varepsilon_F)$ and spin down $\rho_{tot\downarrow}(\varepsilon_F)$ DOS at the Fermi energy are equal, we are not surprised that the polarization of the current is equal to zero. As we go away from the half filling, the difference between spin up and spin down DOS ($\Delta\rho_{tot}(\varepsilon_F) = \rho_{tot\uparrow}(\varepsilon_F) - \rho_{tot\downarrow}(\varepsilon_F)$) starts

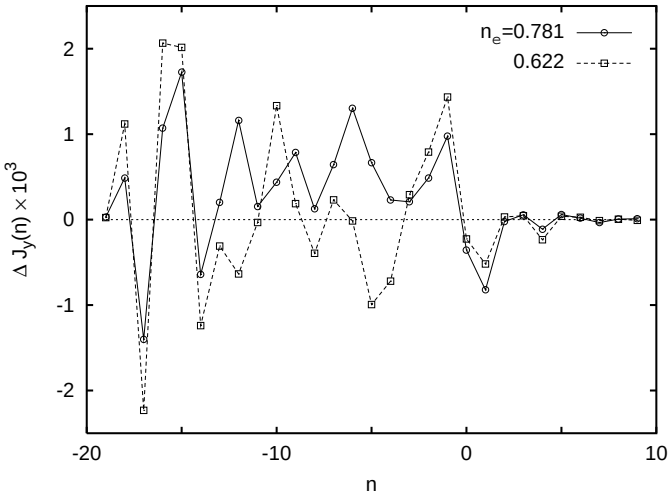

Fig. 14. Spin polarized current $\Delta J_y(n) = J_{y\uparrow}(n) - J_{y\downarrow}(n)$ as a function of the layer index n for exchange splitting $E_{ex} = 0.44$ and concentration of the electrons $n_e = 0.781$ (solid line) and 0.622 (dashed line).

to play a role as it leads to the polarization of the current. A typical example of the polarization of the current $\Delta J_y(n) = J_{y\uparrow}(n) - J_{y\downarrow}(n)$ is shown in Figure 14 for concentration of electrons $n_e = 0.781$ and 0.622. To make the two calculations comparable we have adjusted the parameters so the value of the SC order parameter would be the same. This was achieved by shifting of the coupling constant U_S to -2.129 for $n_e = 0.781$, -2.345 for $n_e = 0.622$ as well as chemical potential to $\mu = -0.5$ and -1.0 respectively.

The total polarization of the current $\Delta J^{tot} = \sum_n J_y(n)$ is of order 10^{-3} and does not depend much on the concentration of electrons n_e. Moreover, we have found a very interesting property of this current, namely, the sign of the polarization of the current depends on whether $n_e < 1$ or > 1. This means, that for $n_e = 1 + x$ we get the same results as for $n_e = 1 - x$, except of the sign of the polarization of the current. This effect can be explained very easily if we recall that polarization of the current is proportional to the difference in the DOS at the Fermi energy, and one can check, that $\Delta\rho_{tot}(\varepsilon_F)$ is an antisymmetric function under the shift $1 - x \to 1 + x$, *i.e.* $\Delta\rho_{tot}(\varepsilon_F, 1 - x) = -\Delta\rho_{tot}(\varepsilon_F, 1 + x)$.

4.6 2D FFLO-like state

Before closing our discussion on the spontaneous current we wish to make a remark regarding the nature of the ground state in our system. To begin with we recall that recently it has been predicted [7,36] that under certain conditions a $3D$-$FFLO$ state is energetically more favorable than the usual $1D$ state. The $3D$ state manifests itself in oscillatory behavior of the pairing amplitude not only in the direction perpendicular to the interface but also in directions parallel to it. Moreover, changing the thickness of the FM slab, one can switch the ground state of the system between the $3D$ and the $1D$-$FFLO$ state [7,36].

The point we wish to make is that the current carrying ground state of our system can be interpreted as a $2D$-$FFLO$ state. The argument is as follows: The oscillations of the pairing amplitude in the direction perpendicular to the interface occur regardless whether the spontaneous current flows or not. Within the $FFLO$ theory [8,9], the period of the oscillations is related to the x-component of the center of mass momentum of the Cooper pair $\mathbf{Q}$. On the FM side of our model the $FFLO$ periodicity is governed by $\mathbf{Q} = (2E_{ex}/v_F)\frac{\mathbf{v}_F}{v_F}$, where $\mathbf{v}_F$ is the Fermi velocity vector, measured with respect to the x axis (see Fig. 1). This can be interpreted as the usual $1D$-$FFLO$ state in confined geometry. On the other hand, when the current flows parallel to the interface, there is a finite vector potential in the y-direction. This can be regarded as a y-component of the $\mathbf{Q}$-vector. So one can say that when the spontaneous current flows, the $2D$-$FFLO$ state is realized. Moreover when the FM thickness is changed the ground state of the system is switched between $2D$- and $1D$-state, which manifests itself in spontaneous current flow or in the lack of it. Clearly this behavior is consistent with the findings of Izyumov *et al.* [36,7]. However in their theory the y-component of $\mathbf{Q}$ remained constant over the whole FM region, vanished in superconductor and was determined by minimizing the total energy of the system. By contrast, in the present calculations this vector was found during the self-consistency procedure, as it is related to the vector potential in the y-direction. Moreover, unlike in references [7,36], the effective Q_y changes its value from layer to layer. Evidently this leads to an inhomogenous $FFLO$-like state in both dimensions.

5 How to observe the current and its polarization?

Clearly, the important issue raised by the above results is "how to observe experimentally the predicted current?" But first of all let's estimate how big this current is. If we assume a bandwidth equal to 1 eV, the average current per layer is of order of tenths of μA. In general the polarization of the ferromagnet can be large, however it cannot be complete. There must be a small number of the minority electrons. In other words it doesn't matter how big the ratio ξ_F/ξ_S is, we should always observe the current. The next point is the thickness of the FM region. Namely, the current is bigger for a thinner sample, but even for thickness of order of several hundreds of ξ_F, we expect the current to be detectable.

Of course, the presence of the current should manifest itself in a number of experiments. For example, since there is a net magnetic flux associated with the current, it could be detected by $SQUID$ experiments or by Hall probes [37]. Another possibility is to measure the conductance across the FM/SC junction [35]. In such experiments the splitting of the zero energy state in the DOS is expected to be observed and, as indicated by equation (22)

the energy distance between the split peaks measures the current flowing. Finally one can also use some local probes like STM techniques to measure the layer resolved DOS.

Confirming that the current is polarized is more troublesome. As we have shown, to get polarized current the system has to be away from the $n_e = 1$ point. In our case, to avoid a Fermi energy mismatch, both the FM and SC are moved from $n_e = 1$. Fortunately, this is only necessary for the ferromagnet. The superconductor can be in a particle-hole symmetric state. In short, realistic estimations of the spin polarization of the spontaneous current require more material specific calculations.

6 Conclusions

In conclusion, we have studied properties of the insulator (or vacuum)-ferromagnet-superconductor trilayer. We have shown, that such a structure supports Andreev bound states forming Andreev bands, whose position can be tuned by thickness of the sample or exchange splitting. Moreover, when a band crosses the Fermi energy, a spontaneous current (and magnetic flux) is generated in the ground state. We have found a relation between the pairing amplitude in the ferromagnet, which has oscillatory behaviour, and the Andreev bound states. Namely, when the Andreev band crosses the Fermi energy the pairing amplitude at the surface opposite to the FM/SC interface changes sign, and as long as current flows it is pinned to zero. The polarization of the current strongly depends on the band filling and is related to the difference in the spin up and spin down density of states at the Fermi level. We also have discussed the question of the supercurrent *vs.* quasiparticle current and gave some experimental clues on how to observe that current. The presented results can be attributed to the $FFLO$ effect influenced Andreev bound states. Finally we would like to stress that the experimental observation of the predicted spontaneous current would constitute a definitive proof of the $FFLO$ nature of the ground state in $I/FM/SC$ heterostructures.

This work has been supported by Computational Magnetoelectronics Research Training Network under Contract No. HPRN-CT-2000-00143. We would like to thank Prof. A. Geim for a usefull conversation regarding the experimental measurability of the magnetic flux associated with the above spontaneous current in the ground state.

References

1. P.M. Tedrow, R. Meservey, Phys. Rep. **238**, 173 (1994); V.T. Petrashov, V.N. Antonov, S.V. Maximov, R. S. Shaikhaidarov, JETP Lett. **59**, 551 (1994); V.T. Petrashov, I.A. Sosnin, I. Cox, A. Parsons, C. Troadec, J. Low Temp. Phys. **118**, 689 (2000); H.-U. Habermeier, G. Cristiani, R.K. Kremer, O. Lebedev, G. van Tendeloo, Physica C **364-365**, 298 (2001)
2. N.F. Berk, J.R. Schrieffer, Phys. Rev. Lett. **17**, 433 (1966); C. Pfleiderer, M. Uhlarz, S.M. Hayden, R. Vollmer, H.v. Lohneysen, N.R. Bernhoeft, G.G. Lonzarich, Nature **412**, 58 (2001); D. Aoki, A. Huxley, E. Ressouche, D. Braithwaite, J. Flouquet, J.-P. Brison, E. Lhotel, C. Paulsen, Nature **413**, 613 (2001)
3. G.E.W. Bauer, Yu.V. Nazarov, D. Huertas-Hernando, A. Brataas, K. Xia, P.J. Kelly, Materials Sci. Eng. B **84**, 31 (2001); S. Oh, D. Youm, M.R. Beasley, Appl. Phys. Lett. **71**, 2376 (1997); L.R. Tagirov, Phys. Rev. Lett. **83**, 2058 (1999)
4. G. Blatter, V.B. Geshkenbein, L.B. Ioffe, Phys. Rev. B **63**, 174511 (2001)
5. C.J. Lambert, R. Raimondi, J. Phys. Cond. Matt. **10**, 901 (1998)
6. A.F. Andreev, Sov. Phys. JETP **19**, 1228 (1964)
7. C.L. Chien, D.H. Reich, J. Magn. Magn. Mater. **200**, 83 (1999); Y.A. Izyumov, Y.N. Proshin, M.G. Khusainov, Phys. Usp. **45**, 109 (2002)
8. P. Fulde, A. Ferrell, Phys. Rev. **135**, A550 (1964)
9. A. Larkin, Y. Ovchinnikov, Sov. Phys. JETP **20** 762 (1965)
10. A.I. Buzdin *et al.*, JETP Lett. **35**, 178 (1982)
11. A.I. Buzdin, M.V. Kuprianov, JETP Lett. **52**, 487 (1990)
12. Z. Radović, M. Ledvij, L. Dobrosavljević-Grujić, A.I. Buzdin, J.C. Clem, Phys. Rev. B **44**, 759 (1991)
13. E.A. Demler, G.B. Arnold, M.R. Beasley, Phys. Rev. B **55**, 15174 (1997)
14. H.K. Wong, B.Y. Jin, H.Q. Yang, J.B. Ketterson, J.E. Hilliard, J. Low Temp. Phys. **63**, 307 (1986); J.S. Jiang, D Davidović, D.H. Reich, C.L. Chien, Phys. Rev. Lett. **74**, 314 (1995); V. Mercaldo, C. Attanasio, C. Coccorese, L. Maritato, S.L. Prischepa, M. Salvato, Phys. Rev. B **53**, 14040 (1996); Th. Mühge, N.N. Garif'yanov, Yu.V. Goryunov, G.G. Khaliullin, L.R. Tagirov, K. Westerholt, I.A. Garifullin, H. Zabel, Phys. Rev. Lett. **77**, 1857 (1996); C.L. Chien, D.H. Reich, J. Magn. Magn. Mater. **200**, 83 (1999)
15. V. Prokić, A.I. Buzdin, L. Dobrosavljević-Grujić, Phys. Rev. B **59**, 587 (1999); A. Kadigrobov, R.I. Shekhter, M. Jonson, Z.G. Ivanov, Phys. Rev. B **60**, 14593 (1999); L. Dobrosavljević-Grujić, R. Zikić, Z. Radović, Physica C **331**, 254 (2000); M. Zareyan, W. Belzig, Yu.V. Nazarov, Phys. Rev. Lett. **86**, 308 (2001)
16. E. Vecino, A. Martin-Rodero, A.L. Yeyati, Phys. Rev. B **64**, 184502 (2001)
17. T. Kontos, M. Aprili, J. Lesueur, X. Grison, Phys. Rev. Lett. **86** 304 (2001)
18. A.I. Buzdin, M.V. Kuprianov, JETP Lett. **53**, 321 (1991); A.I. Buzdin, B. Bujicic, B.M. Yu. Kupriyanov, Sov. Phys. JETP **74**, 124 (1992)
19. G.E. Volovik, L.P. Gor'kov, JETP Lett. **39**, 674 (1984)
20. M. Sigrist, T.M. Rice, K. Ueda, Phys. Rev. Lett. **63**, 1727 (1989)
21. S. Kashiwaya, Y. Tanaka, Rep. Prog. Phys. **63**, 1641 (2000); T. Löfwander, V.S. Shumeiko, G. Wendin, Supercond. Sci. Technol. **14**, R53 (2001)
22. P.G. de Gennes, D. Saint-James, Phys. Lett. **4**, 151 (1963)
23. M. Krawiec, B.L. Györffy, J.F. Annett, Phys. Rev. B **66**, 172505 (2002)
24. I. Turek, V. Drchal, J. Kudrnovský, M. Šob, P. Weinberger, *Electronic Structure of Disordered Alloys, Surfaces and Interfaces* (Kluwer Academic Publishers, Boston, 1997)

25. G. Litak, P. Miller, B.L. Györffy, Physica C **251**, 263 (1995)
26. J.-X. Zhu, C.S. Ting, Phys. Rev. B **61**, 1456 (2000)
27. T. Tokuyasu, J.A. Sauls, D. Rainer, Phys. Rev. B **38**, 8823 (1988)
28. M.J.M. de Jong, C.W.J. Beenakker, Phys. Rev. Lett. **74**, 1657 (1995)
29. K. Halterman, O.T. Valls, Phys. Rev. B **65**, 014509 (2002); Phys. Rev. B **66**, 224516 (2002)
30. A. Bagrets, C. Lacroix, A. Vedyayev, `preprint cond-mat/0112034`
31. K. Kuboki, J. Phys. Soc. Jpn **68**, 3150 (1999)
32. J.A.X. Alexander, T.P. Orlando, D. Rainer, P.M. Tedrow, Phys. Rev. B **31**, 5811 (1985)
33. N.M. Chtchelkatchev, W. Belzig, Yu.V. Nazarov, C. Bruder, JETP Lett. **74**, 323 (2001)
34. A.L. Fauchère, W. Belzig, G.Blatter, Phys. Rev. Lett. **82**, 3336 (1999)
35. S. Kashiwaya, Y. Tanaka, N. Yoshida, M.R. Beasley, Phys. Rev. B **60**, 3572 (1999)
36. Y.A. Izyumov, Y.N. Proshin, M.G. Khusainov, JETP Lett. **71**, 138 (2000); M.G. Khusainov, Y.A. Izyumov, Y.N. Proshin, Physica B **284-288**, 503 (2000)
37. A.K. Geim, S.V. Dubonos, J.G.S. Lok, I.V. Grigorieva, J.C. Maan, L. Theil Hansen, P.E. Lindelof, Appl. Phys. Lett. **71**, 2379 (1997); S.V. Dubnos, A.K. Geim, K.S. Novoselov, I.V. Grigorieva, Phys. Rev. B **65**, 220513 (2002)